1396 *Biochemistry* **2011,** *50,* 1396–1402
DOI: 10.1021/bi101095g

BIOCHEMISTRY
including biophysical chemistry & molecular biology
Article

A Single Nucleotide Polymorphism in Transcobalamin II (I5V) Induces Structural Changes in the Protein As Revealed by Molecular Modeling Studies[†]

Yumnam Silla,[‡,§] Balasubramanian Chandamouli,[‡,§,∥] Souvik Maiti,[‡,⊥] and Shantanu Sengupta*[,‡]

[‡]*Institute of Genomics and Integrative Biology (CSIR), Mall Road, New Delhi, India, and* [⊥]*National Chemical Laboratory (CSIR), Dr. Homi Bhabha Road, Pune, India.* [§]*Both authors contributed equally.* [∥]*Current address: Department of Biology, University of Rome "Tor Vergata", Via della Ricerca Scientifica 1, 00133 Roma, Italy.*

Received July 9, 2010; Revised Manuscript Received December 3, 2010

ABSTRACT: Cobalamin is an essential micronutrient in mammals. Deficiencies of this micronutrient have been implicated as risk factors for various complex diseases. Cobalamin is transported to the cells by the transport protein transcobalamin II (TCII), and hence genetic variations (like single nucleotide polymorphisms) in TCII could be perceived to affect the binding of cobalamin to TCII, thereby modulating the intracellular concentrations of cobalamin. To understand whether three nonsynonymous mutations in TCII (I5V, P241R, and R381Q) alter the structure of the protein which could potentially affect cobalamin binding, we performed molecular dynamics simulation *in silico*. Superimposition of active sites of the four simulated models (wild type and three variants) with the human TCII crystal structure revealed that the distance between the Nε nitrogen atom of His-173 and the cobalt ion of cobalamin deviated considerably in the I5V model as compared to wild type and other variants. His-173 directly coordinates with the cobalt ion of cobalamin. Further, from our dynamic cross-correlation and principal component analysis it appears that in the I5V model the β-domain moves apart from the α-domain creating a wide gap between the two domains. This might facilitate the initial binding of cobalamin in the I5V model as cobalamin enters the binding site through the gap between the two domains. These observations were not found in the other variants. We thus speculate that binding of cobalamin will be more facile in the I5V variant.

Cobalamin (Cbl,[1] vitamin B_{12}), an essential micronutrient, acts as cofactors for the enzymes methionine synthase (methyl-Cbl) and methylmalonyl-CoA mutase (Ado-Cbl) (*1*, *2*). This important micronutrient is only synthesized by microorganisms, and mammals have evolved pathways for absorption, transport, and cellular uptake of Cbl. Cellular uptake of Cbl from diet is mediated by three transport proteins, viz., haptocorrin (HC), intrinsic factor (IF), and transcobalamin II (TCII) (*3*). Initially, Cbl binds to HC in the stomach which after proteolysis in the duodenum binds to IF. Cbl bound to IF is then taken up by mucosal cells in the ileum (*4*). The IF−Cbl complex is then degraded in the enterocyte, and Cbl is transferred to TCII. TCII-bound Cbl is subsequently released in the plasma and is delivered to cells via receptor-mediated endocytosis (*4*, *5*). Only about one-third of Cbl that is bound to TCII (referred to as the biologically active fraction) is taken up by the cells. Although the majority of Cbl is bound to HC in plasma, it does not enter the cells and can be taken up only in the hepatocytes.

Intracellular Cbl deficiency is associated with several disease conditions like megaloblastic anemia, impaired immune defense, and gastrointestinal and neurological disorders (*6*, *7*). Recently, we have shown the association of low vitamin B_{12} levels with coronary artery disease in the Indian population (*8*). Low intracellular vitamin B_{12} concentration may be either due to low intake (especially in individuals adhering to a strict vegetarian diet) or due to defects in absorption, transport, or cellular uptake of the micronutrient. For instance, genetic variations in TCII could affect the binding of vitamin B_{12} to TCII or the recognition of the TC−Cbl complex by the receptor, resulting in lower concentration of intracellular Cbl. Several polymorphisms of TCII have been described. Earlier Afman et al. studied the relationship of nonsynonymous SNPs (in the coding region with total TC concentration) and found that Ile23Val and Pro259Arg seem to affect the binding of vitamin B_{12} (*9*). However, the effect of these coding SNPs on TCII structure has not been studied in detail. Since the crystal structure of TCII has been solved (*10*), effects of these variations on the structure of the protein can be elucidated which may provide clues about binding of Cbl to TCII. The effect of missense mutation or genetic variations on protein structure has previously been demonstrated in a set of disease-causing missense mutations arising from SNPs using molecular modeling studies (*11*). Similarly, the effect of site-directed mutagenesis of phorbol ester binding site in protein kinase (*12*), wild-type and the mutants of phage T4 lysozyme (*13*), energy distribution and fold stability in different fold family proteins (*14*), and human topoisomerase I (*15*) are some of the interesting studies that produced a wealth of data to analyze the internal dynamic behavior of the macromolecules in the presence of the point mutation.

We hypothesized that structural changes in TCII induced by SNPs could lead to alteration in the structure of the protein which

[†]This study was supported by funds provided by the Council of Scientific and Industrial Research (SIP006), India.

*To whom correspondence should be addressed. E-mail: shantanus@igib.res.in. Phone: 91-11-27666156. Fax: 91-11-27667471.

[1]Abbreviations: TCII, transcobalamin II; Cbl, cobalamin; HC, haptocorrin; IF, intrinsic factor; SNP, single nucleotide polymorphism; rmsd, root mean square deviation; rmsf, root mean square fluctuation; ns, nanosecond; DCCM, dynamic cross-correlation map; PCA, principle component analysis.

 Published on Web 01/10/2011

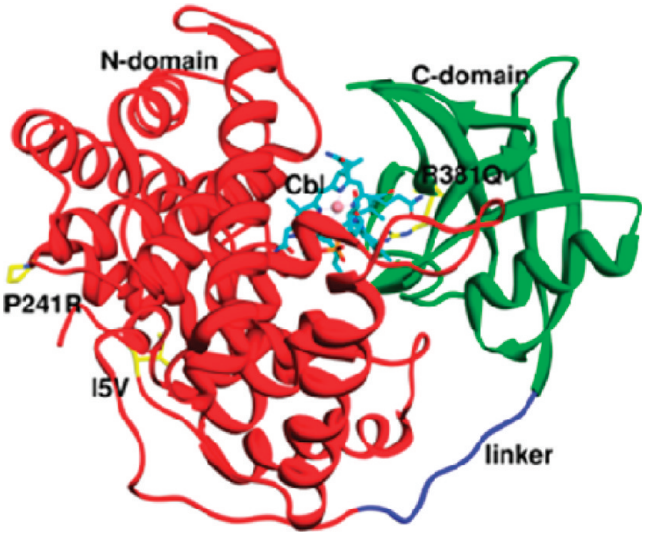

FIGURE 1: Tertiary structure of holo TC. The α- (N-terminal domain) and the β- (C-terminal domain) domains are shown as red spiral ribbons and green arrows, respectively. The linker region is shown in blue. The Cbl (vitamin B_{12}) is represented in cyan in the central domain interface, and positions of the three nonsynonymous SNPs (I5V, P241R, and R381Q) in holo TC are represented in orange.

could potentially affect its binding to Cbl which could potentially lead to modulation of intracellular Cbl concentrations. Thus, in the present work, we analyzed PCA and dynamic cross-correlation to observe changes in the structure of the protein induced by three SNPs [I5V (Ile23Val), P241R (Pro259Arg), and R381Q (Arg399Gln)]. The two SNPs, I5V and P241R, were chosen as several studies have looked at the association of these two polymorphisms with vitamin B_{12}, TCII, and homocysteine concentrations, and the results are controversial (*9*, *16*). The third variation R381Q was taken as of all the variations reported this is closest to the ligand binding site. We found that I5V induces the maximal change in the protein structure which we speculate will lead to more facile binding of Cbl to TCII. We suggest that nonsynonymous mutations in TCII might affect subtle molecular conformational dynamics, thereby leading to altered ligand binding.

MATERIALS AND METHODS

Model Generation. The crystal structure of human TCII obtained from the Protein Data Bank (2bb5) was used to generate the starting models for the simulation (*10*). The structure of holo TC is shown in Figure 1. In holo TC, Cbl is located between the two domains α (N-terminal domain) and β (C-terminal domain) with the plane of the corin ring perpendicular to the domain interface (*10*). After the removal of the Cbl present in the crystal structure, three separate point mutations were introduced into the wild-type crystal structure (Figure 1) that corresponds to the three nonsynonymous SNPs, viz., I5V, P241R, and R381Q, respectively. After mutation, the structure was subjected to optimization using Tripos force field in Sybyl 7.3. Four different simulations were carried out that include the wild type and the three mutated models, I5V, P241R, and R381Q, and each system was simulated for 22 ns.

Simulation. All simulations were carried using Amber9 (*17*) with ff99SB force field (*18*) and with periodic boundary conditions. The starting models were neutralized with potassium ions and were then immersed in a periodic box of TIP3P water model (*19*), which extended to 12 Å from the solute. The particle mesh Ewald method was used to treat the long-range electrostatics (*20*). Bond lengths involving bonds to hydrogen(s) were constrained using SHAKE algorithm (*21*). A time step of 2 fs was used. The conformational sampling was done at a constant pressure of 1 atm and a temperature of 300 K. Langevin coupling with a collision frequency of 1.0 was used for temperature regulation (*22*). The equilibration procedure involves (1) two rounds of minimizations (1500 iterations each) and dynamics (25 ps each) of the solvent and potassium ions in the bulk solvent keeping the solute constrained to its initial position with decreasing force constants of 500, 100, 300, and 50 kcal/(mol Å^2), (2) four rounds of 2000 steps of minimization of the whole system where the solute restraint was kept as 100, 50, 25, and 5 kcal/(mol Å^2), and (3) an unrestrained minimization of the whole system. Finally, the system was heated to 300 K at constant volume and equilibrated for 300 ps at constant pressure. The production phase

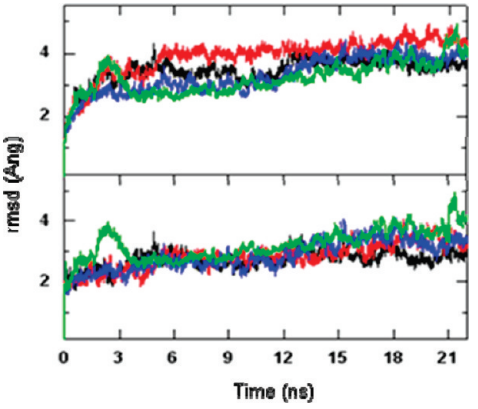

FIGURE 2: Plots representing the stability of the models during the dynamics runs. The root mean square deviation of the backbone atoms from the starting structure as a function of simulation time is shown in the upper panel, and rmsd calculated with respect to the average structure is shown in the lower panel. The models are represented as wild type, I5V, P241R, and R381Q in black, red, blue, and green, respectively.

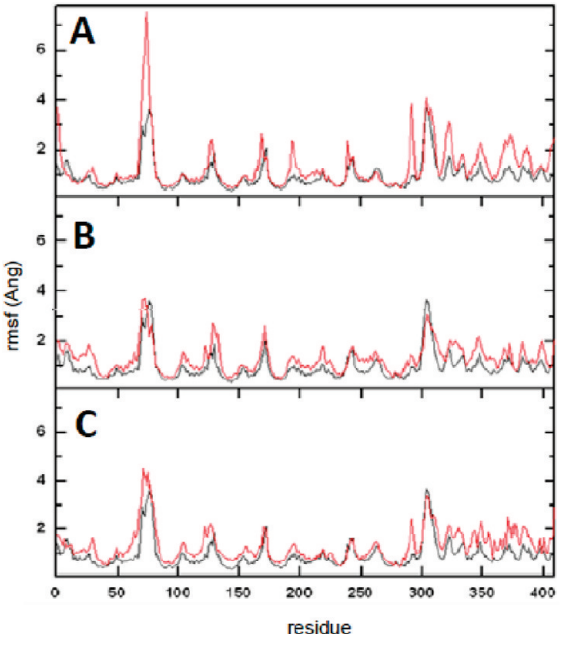

FIGURE 3: Root mean square fluctuation (rmsf) of residues as a function of residue number. Wild type is shown in black. The mutated data are shown in red in all of the variants and represented as (A) I5V, (B) P241R, and (C) R381Q, respectively.

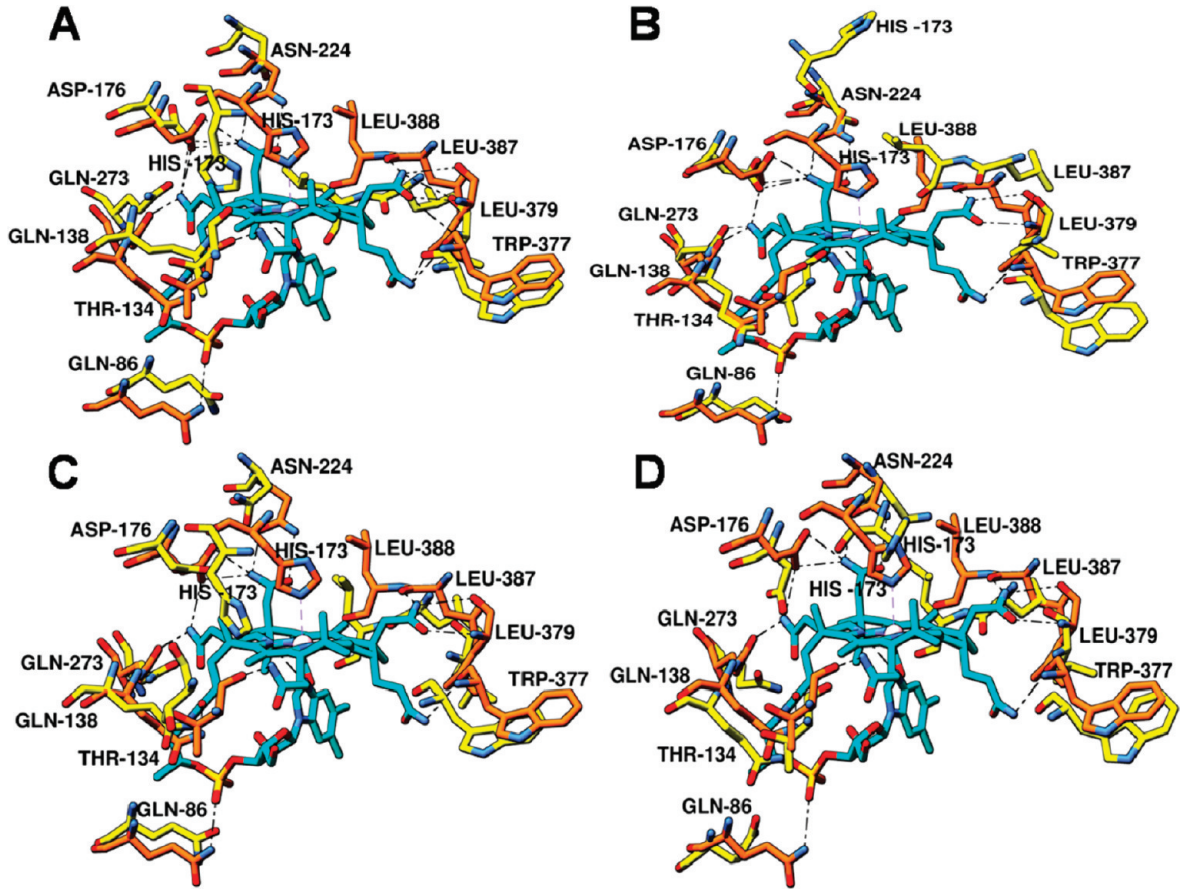

FIGURE 4: Superimposition of active sites. TCII crystal structure is depicted in orange, and simulated structures are shown in yellow as (A) wild type, (B) I5V, (C) P241R, and (D) R381Q model, respectively. Cbl is represented in cyan that coordinates with the upper His-173 residue, and the central Co atom is depicted as a pink sphere. N and O atoms are drawn in blue and red, respectively. H-atoms have been removed for clarity in all of the models. All of the residues which are in direct H-bond to the Cbl are labeled.

was started at this stage, and the conformations were collected in the trajectories at intervals of 2 ps.

Analysis. The root mean square deviation (rmsd) and root mean square fluctuation (rmsf) analysis was done with PTRAJ program. The dynamic correlation analysis was done with bio3d package (*23*), taking the cross-correlation coefficient for C_α atom displacement for each model MD trajectory. The cross-correlation coefficients (C_{ij}) were computed as

$$C_{ij} = \frac{\langle \Delta r_i \Delta r_j \rangle}{\sqrt{\langle \Delta r_i^2 \rangle}\sqrt{\langle \Delta r_j^2 \rangle}} \quad (1)$$

where Δr_i is the description from the mean position of the C_α atom in the ith residue. The broken brackets represent the time average over the whole trajectory (*23*, *24*). The positive C_{ij} values indicate the correlated motions in the same directions. The negative values of C_{ij} represent an anticorrelated motion between the residues. The principal component analysis was done on the backbone C_α atoms of the protein using pcazip software (*25*) based on the covariance matrix:

$$C_{ij} = \left\langle (r_i(t) - \langle r_i \rangle_t)(r_j(t) - \langle r_j \rangle_t) \right\rangle_t \quad (2)$$

where r_i, r_j are the Cartesian coordinates of the ith and jth atoms, respectively, the covariance eigenvector and eigenvalues defined the collective dynamic mode and amount of variance movement (*26*−*28*), and t represents the average time over the whole MD trajectory. The figures were generated with chimera (*29*).

RESULTS

Structural Flexibility. The stability of the simulations was monitored by calculating the root mean square deviation from the starting models. The plot of rmsd as a function of simulation time is reported in Figure 2. The rmsd of all the models increased initially due to the relaxation of the models from the starting configuration. The rmsd of the models I5V (red) and P241R (blue) reached a plateau after 2 ns while the rmsd of the wild type (black) and R381Q (green) reached after 4 ns. The simulations were done up to 22 ns, and all of the following analysis was carried out on the last 17 ns of the trajectory, where the protein reaches a stable structure in all simulations. The rmsd of all the backbone atoms of the α-domain, β-domain, and linker region as a function of simulation time in each model is shown in Supporting Information Figure S1. To identify the regions of higher flexibility, the per residue root mean square fluctuation (rmsf) was calculated as shown in Figure 3. The rmsf of the wild type is shown in black, while that of the mutated models is shown in red. The rmsf of the mutated models were found to be similar to that of wild type. However, in I5V a large fluctuation (>7 Å) is observed, encompassing residues 68−78 that include the loop region in the α-domain.

Active Site Orientation. It has been reported earlier that there are two types of strong interaction between cobalamin and TCII (*10*). The first is the coordination bond between Co and a side chain of His-173, while the second interaction is the hydrogen bonds linking Cbl to TCII (*10*). To see the effect of mutation on the active site residue orientation, we superimposed

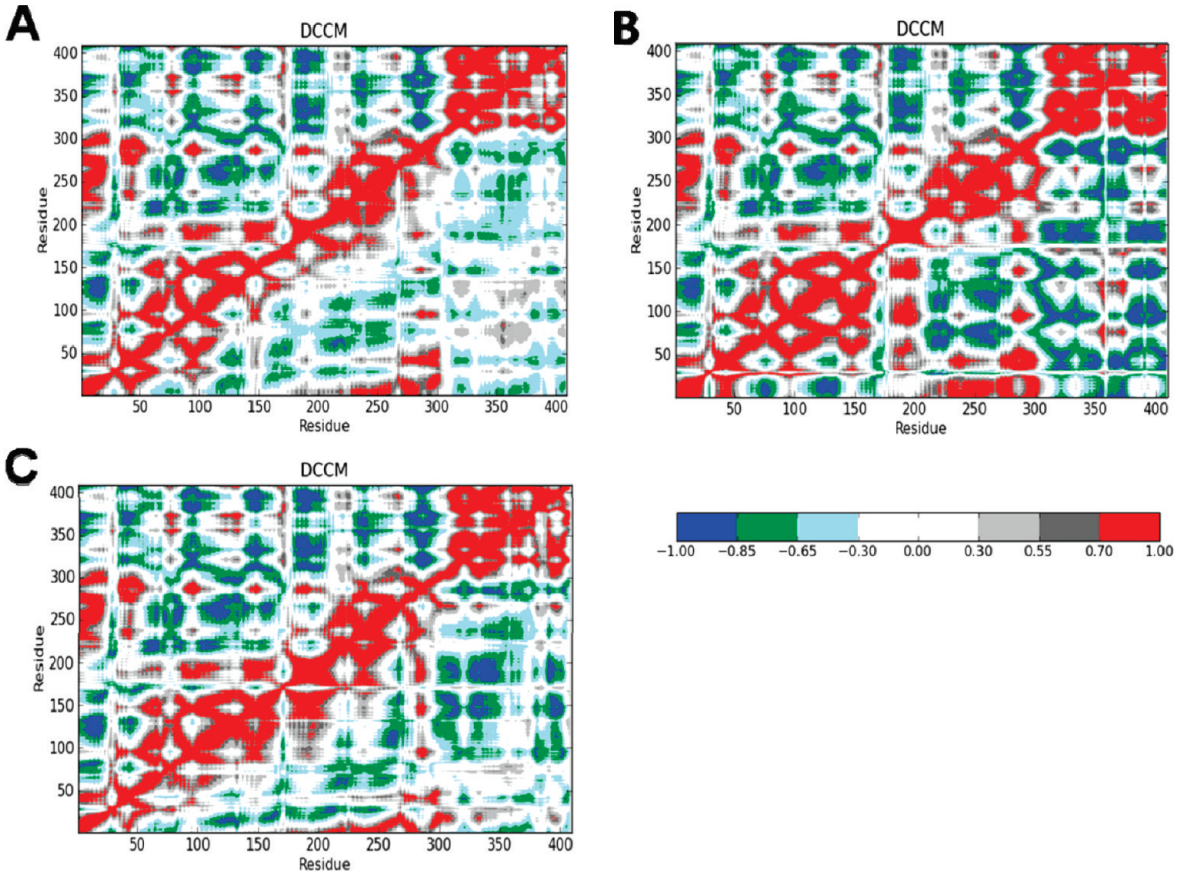

FIGURE 5: Residue-based correlated motions (dynamic cross-correlation map) calculated for all of the C_α atoms in wild type and variant models, using the last 17 ns of time average. Regions colored in red represent the strong correlation motion while blue represents the anticorrelated regions. In each figure the upper panel represents the wild-type structure. The lower panels represent I5V (A), P241R (B), and R381Q (C) variant.

the structures obtained from simulation on the crystal structure. The residues that are involved in direct hydrogen bonds with Cbl include Gln-86, Thr-134, Gln-138, Asp-176, Asn-224, Gln-273, Leu-358, Leu-363, Trp-377, Leu-379, Leu-387, and Leu-388 (*10*). A close-up view of the active site is shown in Figure 4 from which it is evident that the orientations of all the residues involved in direct hydrogen bond with Cbl do not deviate to an appreciable extent in the simulated models when compared to the crystal structure. In contrast, the orientation of the His-173, which is directly coordinated to the Co ion of Cbl, is altered to an appreciable extent in the I5V model. The distance between the Nε nitrogen atom of His-173 and the Co ion of Cbl which is 2.8 Å in the crystal structure deviated to approximately ~14.7 Å in I5V model (Figure 4B). However, in the other simulated models the distances between the Nε nitrogen atom of His-173 and the Co ion of Cbl were ~4.7 Å in the wild type, 5.2 Å in the P241R model, and ~5.6 Å in the R381Q model (Figure 4A,C,D). The increased deviation of His-173 orientation in I5V could facilitate the initial binding of the ligand.

Dynamic Cross-Correlation Map. The dynamic cross-correlation map (DCCM) was analyzed to understand the changes in correlated motion induced by the single amino acid substitution in protein. The analysis provided a comprehensive picture of the correlated motions which is represented in Figure 5. The regions colored in blue are significantly anticorrelated while the regions colored in red are indicative of strong correlation between the movements of residues. In the wild-type correlation map (Figure 5, upper panels) we observed a strong positive correlation between residues 1−23, 44−49, 143−152, 188−197, and 223−300 in the α-domain. These regions correspond to the helices that form a part of the inner core of the α-domain (*10*) close to the side opposite to the *β*-domain. In contrast to wild type, this portion of the protein behaves differently in the I5V model (Figure 5A, lower panel). In this case, the correlation in the α-domain was restricted between residues 248−256 and 272−301, and the strong correlation of residues in the inner core of the α-domain was not observed. Further, the anticorrelated motions were significantly different between wild type and I5V. In wild type there are several residues like 118−147 with 3−20 and 250−277 with 102−150 in the α-domain that are strongly anticorrelated. However, these regions are not strongly anticorrelated in the I5V structure. Similarly, the regions in the *β*-domain encompassing residues 305−347 and 376−408 [including the linker region of 9 residues (301−309)] were found to be anticorrelated with residues 177−202, 275−294, and 140−150 in the wild-type model which was not the case in the I5V model. In the P241R (Figure 5B, lower panel) the strong correlated and anticorrelated motions between intra- and interdomain regions observed were similar to wild type (Figure 5B, upper panel) and differed from that of I5V. We also did not observe significant difference between wild type and the R381Q model (Figure 5C, upper and lower panels, respectively).

PCA Analysis. In order to identify the overall pattern of protein motion, we carried out PCA analysis on the C_α atoms. The technique helps to identify the total concerted motion of the atoms in the protein expressed by the eigenvectors of the covariance matix which is implied by its corresponding eigen values (*25*, *27*). The frequency of the eigenvectors with large

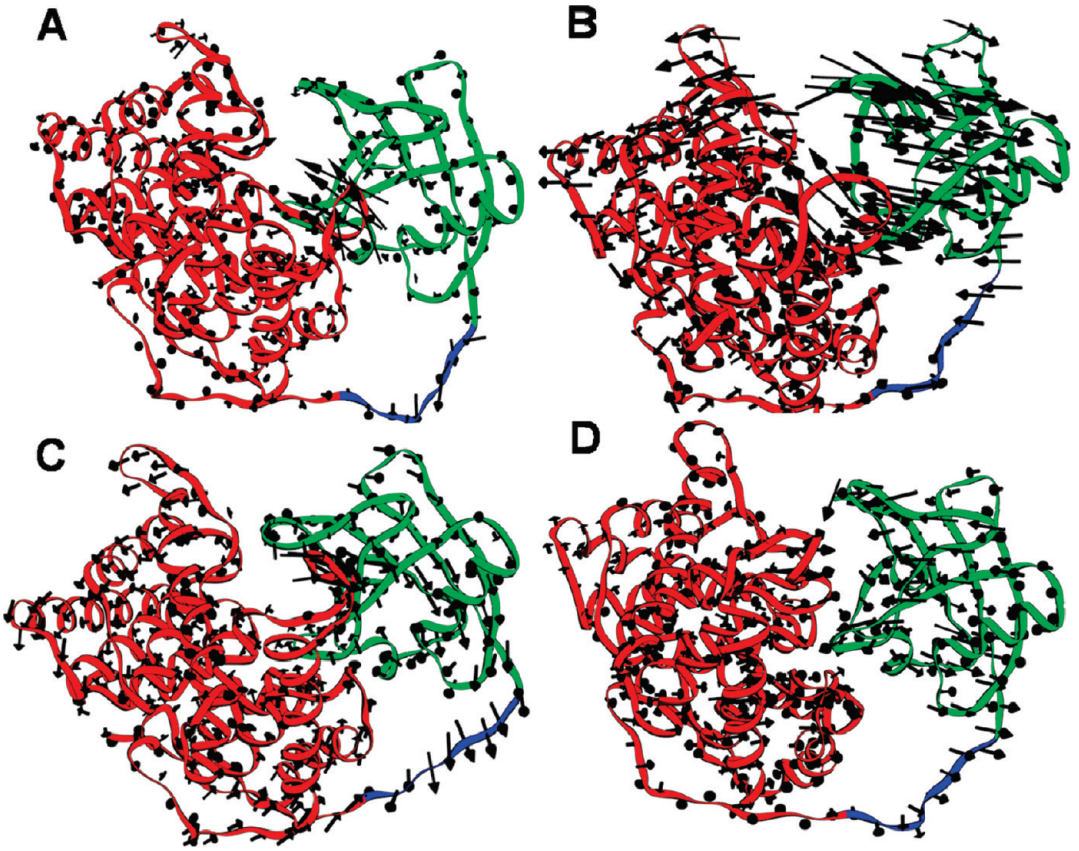

FIGURE 6: Porcupine plots obtained from the first eigenvector of TCII wild type and variant model MD motions produced by principal component analysis. The models are shown as (A) wild type, (B) I5V, (C) P241R, and (D) R381Q, respectively. The arrows in the structures indicate the direction of motions where the majority of the protein motion occurred. In each model the N-terminal domain (α-domain) is displayed in red and the C-terminal domain (*β*-domain) in green. The linker region is represented in blue.

eigenvalues can usually represent the total concerted motion of the protein correlated to the protein function (*26*, *28*). The cumulative sum of eigenvalues as a function of number of eigenvalues derived from the trajectory collected at the last 17 ns is shown in Supporting Information Figure S2. The motion of the protein along the first eigenvector is depicted in Figure 6. In the wild type, the most fluctuating part is in the loop region (68−78) and the linker region (301−309). Major domain motion was not observed in wild type as seen from the figure. The least domain motion occurred within the residues in the α- and *β*-domain (Figure 6A). This pattern was also observed in P241R and R381Q models (Figure 6C,D). However, in contrast to other models, in I5V the arrows in the porcupine plot (Figure 6B) clearly indicate that the residues that constitute the α-domain move in a direction opposite to the *β*-domain residues that can result in the opening of the active site. The second and third eigenvector porcupine plots of all four models are shown in the Supporting Information Figure S3. As can be seen from the figures the maximum fluctuation is observed from the first eigenvector.

DISCUSSION

A third of the total Cbl binds to TCII, and this complex (holo transcobalmin II) is considered to be the biologically active form as this determines the intracellular Cbl concentration. There are conflicting results regarding the association of single nucleotide polymorphism in the TCII genes [especially 776C > G (P241R)] with the level of holo TCII and vitamin B_{12}. Some studies reported significant association of 776C > G polymorphism with holo TCII and B_{12} levels (*30*−*32*), while others clearly show that there is no association between allelic variations of 776C > G with plasma B_{12} level (*9*, *16*). Since the crystal structure of TCII has been deciphered, we performed molecular dynamics simulation studies with the wild type and three coding SNPs (I5V, P241R, and R381Q) to ascertain the effect of these variations on the structure of TCII and ascertain if this could potentially affect B_{12} binding.

It has been reported in the crystal structure that His-173 directly coordinates to Cbl via its imidazole Nε atom. Superimposition of the active site regions of the crystal structure and our simulated structures with the variants revealed that only in the I5V model the orientation of His-173 deviated considerably from the original crystal structure. This His-173 has been reported to be at the end of the flexible loop preceding the inner helix close to the Cbl (*10*). The deviation of His-173 in I5V might lead to more flexibility in this region. Kinetic studies have shown that the binding of Cbl to TC occurs in two steps. The initial attachment is to an open conformation of the protein which is followed by transition to a closed state. This transition leads to the displacement of water in Cbl in Cbl-OH_2 by protein residue histidine (*33*, *34*). From our DCCM results we found that the strong correlation at the core of the α-domain (1−23, 44−49, 143−152, and 188−197) in wild type and the other two models (P241R and R381Q) was absent in the I5V model. Similarly, in wild type, the strong anticorrelated region in the α-domain is in contrast to the I5V, where it is least anticorrelated. Further, from our PCA results it is clear that in the I5V model the residues that are involved in the C-terminal domain move in a direction

opposite to the N-terminal domain residues. This might facilitate the initial binding of Cbl in the I5V model as Cbl cannot enter the binding site without an initial gap between the two domains, and our results indicate that this gap may be wider in I5V than that in wild type and the other variant model. A linker region of 9 residues (301−309) maintains the position of these two domains. With significant protein motion within domain−domain interaction in I5V, the flexibility of this linker region will be more, which indicates that the entry of Cbl will be more facile. Interestingly, human intrinsic factor (IF) and TCI (HC), the two other Cbl binding proteins, code for valine in this position instead of isoleucine in TCII (*35*). Also, Afman et al. suggested that heterozygosity for the I5V (I23V) variant leads to higher proportion of vitamin B_{12} bound to TC (*9*) further indicating our findings.

In contrast to the I5V variation, our structural studies with P241R revealed marginal deviation of His-173 when compared to the wild-type structure. Further, in DCCM the correlated motion in this variation was similar to the wild type. This was also supported by the PCA analysis which indicated that no substantial motional changes between the two domains were induced by P241R variation. The variant P241R is the most common polymorphism in the TCII gene, and most of the association studies done to date involve this SNP. It had been reported earlier that this variation could alter secondary structure of this protein (*36*), and hence it was speculated that it could potentially alter the protein's ability to deliver Cbl to the cells leading to vitamin B_{12} deficiency. In tune with this some studies clearly show association of this polymorphism with holo TC and vitamin B_{12} levels (*30*−*32*). However, there are several other studies which did not find any such association (*9*, *16*). Our structural studies indicating that this polymorphism may not affect the binding of Cbl to TCII corroborate the finding of Wuerges et al. (*10*), who clearly showed from the crystal structure that P241R is in the flexible loop between helices and hence suggested that the P241R polymorphism will not influence the binding of Cbl to TCII. They also mention that the role of this substitution in binding of holo TCII to its receptor is also unlikely due to high sequence variability among the seven mammalian TCs in the vicinity of the polymorphism. Apart from this variation we also did not find any major structural changes with the R381Q variation.

In conclusion, our current structural analysis suggests that in the I5V model the local changes at the Cbl binding site probably affect the protein domain motion thus promoting the initial binding of Cbl between the domain interface. It would be interesting to investigate the effect of the I5V variation with respect to Cbl's binding to TC under physiological condition in future studies.

ACKNOWLEDGMENT

The authors thank Dr. Elayanambi Sundaramoorthy, Dr. Bhupesh Taneja, and Dr. Kaushik Chakraborty for valuable suggestions.

SUPPORTING INFORMATION AVAILABLE

Results showing the rmsd of domain and linker regions from the starting structure with respect to the function of simulation time (Figure S1), cumulative eigenvector contribution to the total protein motion (Figure S2), and porcupine plots of the second and third eigenvector obtained from the principal component analysis (Figure S3). This material is available free of charge via the Internet at http://pubs.acs.org.

REFERENCES

1. Drennan, C. L., Huang, S., Drummond, J. T., Matthews, R. G., and Ludwig, M. L. (1994) How a protein binds B-12: a 3.0-angstrom X-ray structure of B-12 binding domains of methionine synthase. *Science 266*, 1669–1674.
2. Banerjee, R., and Ragsdale, S. W. (2003) The many faces of vitamin B12: catalysis by cobalamin-dependent enzymes. *Annu. Rev. Biochem. 72*, 209–247.
3. Seetharam, B., and Alpers, D. H. (1982) Absorption and transport of cobalamin (vitamin B12). *Annu. Rev. Nutr. 2*, 343–369.
4. Quadros, E. V., Regec, A. L., Kahn, K. M., Quadros, E., and Rothenberg, S. P. (1999) Transcobalamin II synthesized in the intestinal villi facilitates transfer of cobalamin to the portal blood. *Am. J. Physiol. 277*, 161–166.
5. Seetharam, B. (1999) Receptor-mediated endocytosis of cobalamin (vitamin B12). *Annu. Rev. Nutr. 19*, 173–195.
6. Tuchman, M., Kelly, P., Watkins, D., and Rosenblatt, D. (1998) Vitamin B12-responsive megaloblastic anemia, homocystinuria, and transient methylmalonic aciduria in cbIE disease. *J. Pediatr. 113*, 1052–1056.
7. Cooper, B., and Rosenblatt, D. (1987) Inherited defects of vitamin B-12 metabolism. *Annu. Rev. Nutr. 7*, 291–320.
8. Kumar, J., Garg, G., Sundaramoorthy, E., Prasad, P. V., and Karthikeyan, G. (2009) Vitamin B12 deficiency is associated with coronary artery disease in an Indian population. *Clin. Chem. Lab. Med. 47*, 334–338.
9. Afman, L. A., Lievers, K. J. A., Van Der Put, N., Trijbels, F. J. M, and Blom, H. J. (2002) Single nucleotide polymorphisms in the transcobalamin gene: relationship with transcobalamin concentrations and risk for neural tube defects. *Eur. J. Hum. Genet. 10*, 433–438.
10. Wuerges, J., Garau, G., Geremia, S., Fedosov, S. N., Petersen, T. E., and Randaccio, L. (2006) Structural basis for mammalian vitamin B_{12} transport by transcobalamin. *Proc. Natl. Acad. Sci. U.S.A. 103*, 4386–4391.
11. Wang, Z., and Moult, J. (2001) SNPs, protein structure and human disease. *Hum. Genet. 17*, 263–270.
12. Wang, S., Kazanietz, M. G., Blumberg, P. M., Marquez, V. E., and Milne, G. W. A. (1996) Molecular modeling and site-directed mutagenesis studies of a phorbol ester-binding site in protein kinase C. *J. Med. Chem. 39*, 2541–2553.
13. Lee, J., Lee, K., and Shin, S. (2000) Theoretical studies of the response of a protein structure to cavity-creating mutations. *Biophys. J. 78*, 1665–1671.
14. Morra, G., and Colombo, G. (2008) Relationship between energy distribution and fold stability: insights from molecular dynamics simulations of native and mutant proteins. *Proteins 72*, 660–672.
15. Chillemi, G., Fiorani, P., Benedetti, P., and Desider, A. (2003) Protein concerted motions in the DNA-human topoisomerase I complex. *Nucleic Acids Res. 31*, 1525–535.
16. Sunder-Plassmann, G., and Födinger, M (2003) Genetic determinants of the homocysteine level. *Kidney Int. 63*, S141–S144.
17. Case, D. A., Cheatham, T., Darden, T., Gohlke, H., Luo, R., Merz, K. M., Jr., Onufriev, A., Simmerling, C., Wang, B., and Woods, R. (2005) The Amber biomolecular simulation programs. *J. Comput. Chem. 26*, 1668–1688.
18. Hornak, V., Abel, R., Okur, A., Strockbine, B., Roitberg, A., and Simmerling, C. (2006) Comparison of multiple Amber force fields and development of improved protein backbone parameters. *Proteins 65*, 712–725.
19. Jorgensen, W. L., Chandrasekhar, J., Madura, J. D., Impey, R. W., and Klein, M. L. (1983) Comparison of simple potential functions for simulating liquid water. *J. Chem. Phys. 79*, 926–935.
20. Darden, T., York, D., and Pedersen, L. (1993) Particle mesh Ewald-Ann.log (n) method for ewald sums in large systems. *J. Chem. Phys. 98*, 10089–10092.
21. Ryckaert, J. P., Ciccotti, G., and Berendsen., H. J. C. (1977) Numerical integration of the Cartesian equations of motion of a system with constraints: molecular dynamics of n-alkanes. *J. Comput. Phys. 23*, 327–341.
22. Izaguirre, J. A., Catarello, D. P., Wozniak, J. M., and Skeel., R. D. (2001) Langevin stabilization of molecular dynamics. *J. Chem. Phys. 114*, 2090–2098.
23. Grant, B. J., Rodrigues, A. P. C., ElSawy, K. M., McCammon, J. A., and Caves., L. S. D. (2006) Bio3d: an R package for the comparative analysis of protein structures. *Bioinformatics 22*, 2695–2696.
24. McCammon, J. A., and Harvey, S. C. (1987) Dynamics of Proteins and Nucleic Acids, Cambridge University Press, Cambridge.
25. Mayer.; et al. (2006) Pcazip compresses trajectory files using the PCA method. *J. Chem. Theor. Comp. 2*, 251–258.

26. Amadei, A., Linssen, A. B. M., and Berendsen, H. J. C. (1993) Essential dynamics of protein. *Proteins 17* (4), 412–25.
27. Garcia, A. E. (1992) Large-amplitude non-linear motions in proteins. *Phys. Rev. Lett. 68*, 2696–2700.
28. Balsera, M., Wriggers, W., Oono, Y., and Schulten, K. (1996) Principal component analysis and long time protein dynamics. *J. Phys. Chem. 100*, 2567–2572.
29. Pettersen, E. F., Goddard, T. D., Huang, C. C., Couch, G. S., Greenblatt, D. M., Meng, E. C., and Ferrin, T. E. (2004) UCSF chimera—a visualization system for exploratory research and analysis. *J. Comput. Chem. 25*, 1605–1612.
30. Zetterberg, N. E., and Regland, B. B. (2003) The transcobalamin (TC) codon 259 genetic polymorphism influences holo-TC concentration in cerebrospinal fluid from patients with Alzheimer disease. *Clin. Chem. 49*, 1195–1198.
31. Lievers, K. J. A., Afman, L. A., Kluijtmans, L. A. J., Boers, G. H. J., Verhoef, P., den Heijer, M., Trijbels, F. J. M., and Blom, H. J. (2002) Polymorphisms in the transcobalamin gene: association with plasma homocysteine healthy individuals and vascular disease patients. *Clin. Chem. 48*, 1383–1389.
32. Swanson, D. A., Pangilianan, F., Mills, J. L., Kirke, P. N., Conley, M., Weiler, A., Frey, T., Parle-McDermott, A., O'Leary, V. B., and Seltzer, R. R. (2005) Evaluation of transcobalamin II polymorphisms as neural tube defect risk factors in an Irish population. *Birth Defects Res. Part A 73*, 239–244.
33. Fedosov, S. N., Berglund, L., Fedosova, N. U., Nexø, E., and Petersen, T. E. (2002) Comparative analysis of cobalamin binding kinetics and ligand protection for intrinsic factor, transcobalamin and haptocorin. *J. Biol. Chem. 277*, 9989–9996.
34. Fedosov, S. N., Fedosova, N. U., Nexø, E., and Petersen, T. E. (2000) Conformational changes of transcobalamin induced by aquocobalamin binding. *J. Biol. Chem. 275*, 11791–11798.
35. Li, N., Seetharam, S., and Seetharam, B. (1995) Genomic structure of human transcobalamin II: comparison to human intrinsic factor and transcobalamin I. *Biochem. Biophys. Res. 17*, 756–764.
36. Li, N., Sood, G. K., Seetharam, S., and Seetharam., B. (1994) Polymorphism of human transcobalamin II: substitution of proline and/or glutamine residues by arginine. *Biochim. Biophys. Acta 1219*, 515–520.